CHEMICAL ENGINEERING TRANSACTIONS
VOL. 106, 2023
A publication of AIDIC
The Italian Association of Chemical Engineering
Online at www.cetjournal.it
Guest Editors: Jeng Shiun Lim, Nor Alafiza Yunus, Peck Loo Kiew, Hon Huin Chin

ISBN 979-12-81206-05-2; **ISSN** 2283-9216
DOI: 10.3303/CET23106226

Efficient Degradation of Textile Wastewater Over $CaFe_2O_4$ Photocatalyst Under Visible Light

Emyra Ezzaty Masiren[a], Huei Ruey Ong[a,*], Md. Maksudur Rahman Khan[b]

[a]Faculty of Engineering & Technology, DRB- HICOM University of Automotive Malaysia, Peramu Jaya Industrial Area, 26607 Pekan, Pahang, Malaysia
[b]Petroleum and Chemical Engineering Programme area, Universiti Technology Brunei, Gadong, Brunei Darussalam
roi_rui86@hotmail.com

A critical global problem is the excessive release of textile effluent that contains the organic compound Methylene Blue (MB) dye into the environment. It harms the environment and living things due to its persistence and toxicity. For instance, it has an impact on birth weight and prenatal neurodevelopment. By now, photocatalytic degradation is a rapidly developing, effective, and energy-saving method for eliminating organic pollutants from the aquatic environment. Using a wet chemical procedure (the sol-gel technique), Calcium iron oxide ($CaFe_2O_4$) was synthesized. Some characterization findings show that the $CaFe_2O_4$ Powder X-ray diffraction (XRD) pattern is well suited to the orthorhombic structure. Thermogravimetric (TG) analysis research revealed that at around 700°C, the overall weight losses for high-temperature calcined samples started to decline steadily. The $CaFe_2O_4$ powder samples calcined at 700°C show more substantial typical band gaps of 2 eV for their UV-vis absorption characteristics. The $CaFe_2O_4$ sample that has been developed exhibits remarkable photocatalytic capability. The photocatalytic activity was measured by how quickly MB broke down when exposed to visible light. Investigated were the effects of the photocatalyst's calcination temperatures and starting concentration. The acquired experimental results showed that the synthesized $CaFe_2O_4$ photocatalyst could use visible light irradiation to degrade more than 50% of the dye in an aqueous solution.

1. Introduction

Researchers are creating enzymes to degrade toxic water pollution (Phakathi et al., 2022). The textile, printing, and dyeing industries pollute water sources (Benites-Alfaro et al., 2022). The textile industry is highly chemically intensive. The dye contains heavy metals, ions, organic halogens, and color (Bidu et al., 2023). MB is a pollutant found in fabrics, silk, and wood. Redox indicators, biological stains, and pharmaceutical dyes damaged the gastrointestinal, genitourinary, and cardiovascular systems, creating massive amounts of non-biodegradable organic and inorganic waste (Kukwa & Chetty, 2022). The material is hazardous and may cause pollution. Textile colors reduce oxygen and light penetration (Jayalakshmi et al., 2022). Research must address this issue. Semiconducting catalysts remove water pollutants without killing themselves in a photocatalytic breakdown. Photocatalysis includes light-induced electron-hole pair production (Aslam et al., 2022). The catalyst creates holes by transferring electrons from the valence to the conduction band. Photogenerated electrons and holes create reactive chemical species that degrade solution toxins (Sánchez-Albores et al., 2022). The catalyst's surface area and active spots increase the organic dye charge carriers and free radical species (Antony et al., 2023). References show metal oxide nano-catalyst processes. Photocatalysis is best done using iron oxide nanoparticles (Glazkova et al., 2022). Metal oxides with visible light active band gaps absorb 43% of the solar spectrum, making them superior photocatalysts (Kousar et al., 2022). Because of its unique properties, spinel ferrite may decay in dirty water. Iron-based materials are becoming more common because iron elements are common in the earth's crust. These materials are used as co-catalysts or catalyst carriers in several processes (Khosroshahi et al., 2022). The $CaFe_2O_4$/PMS/Vis system was investigated for its ability to remove other pollutants such as antibiotics (tetracycline, ciprofloxacin) and dye (sunset yellow) and degradation up to 77% (Tuna & Simsek, 2023). Thus, adding $CaFe_2O_4$ to textile effluent is an intriguing study issue. Researchers are interested in the low-cost, chemically stable, narrow-band p-type gap material $CaFe_2O_4$. Large-scale

Paper Received: 19 April 2023; Revised: 25 August 2023; Accepted: 12 October 2023
Please cite this article as: Masiren E.E., Ong H.R., Khan M.M.R., 2023, Efficient Degradation of Textile Wastewater Over CaFe2O4 Photocatalyst Under Visible Light, Chemical Engineering Transactions, 106, 1351-1356 DOI:10.3303/CET23106226

photocatalytic wastewater treatment has sought highly visible, light-responsive photocatalysts (Jarusheh et al., 2022). Photo-degradation requires a sol-gel-prepared nanoscale $CaFe_2O_4$ photocatalyst. This method is helpful because process factors can rapidly alter to produce oxide pellets with different values (Kamali et al., 2021). $CaFe_2O_4$ photocatalyst degraded MB dye under xenon bulb visible light. The $CaFe_2O_4$ nanoparticles that adsorbed to the dye molecules reduced the pollutants by up to 86%(Keerthana et al., 2022). Dye molecules were relatively broken down. Sol-gel produced a $CaFe_2O_4$ heterogeneous structure for photocatalytic pollutant degradation. X-ray diffraction analysis (XRD), UV-Vis Spectroscopy and thermal gravimetric analysis (TGA) were used to characterize the catalyst. Photo-degradation requires a visible-light active reagent. The objective is to produce a photoreactive catalyst for the photooxidative decomposition of organic compounds. The effects of the photocatalyst's initial concentration and calcination temperatures were examined. $CaFe_2O_4$, as one of the coloring ingredients in textile effluent, is the research that needs to be addressed by this study. The newly created visible light response catalyst is anticipated to be one of the feasible solutions for the textile photo-degradation process.

2. Experimental

2.1 Formation of $CaFe_2O_4$

The sol-gel technique was used in the synthesis of $CaFe_2O_4$ nanoparticles. For the preparation of the precursors, analytical-grade Calcium nitrate tetrahydrate and iron (III) nitrate were acquired from Loba Chemical. In a volume of 100 mL of a 30% ammonia solution containing deionized water, the metal salts calcium and iron were combined in a molar ratio of 1:2. After that, the solution was heated gradually up to 80°C while being continuously stirred. Then 5 ml of ethylene glycol was added to the mixture. The solution produced was held at a temperature of 120°C with constant stirring until it changed into a xerogel. The gel fully evaporated when heated further, turning into a powdery substance instead. $CaFe_2O_4$ photocatalyst powder was obtained by calcining the brown, desiccated, gel-like mixture produced by the reaction at 450 °C for 2 h. After that, the temperature was increased to 700 °C, 800 °C, 900 °C, and 1,050 °C for 10 h. A portion of the freshly synthesized powder was annealed in its entirety for a total of eight hours at a range of temperatures. Then, $CaFe_2O_4$ powders were ground in a mortar.

2.2 Characterization of Samples

The goal of characterising a catalyst's physical features was to help researcher better understand its structural reactivity and physical characteristics. XRD analysis was performed using a Panalytical X-ray diffractometer with Cu K radiation in the 10-80 range to assess the crystal phases of materials. TGA analysis using a Shimadzu DTG-60H instrument. The samples were heated in an oxidising atmosphere (synthetic air with 21% O_2 and 79% N_2) at a rate of three °C/min from 25 to 1,000 °C. The ES-300 photoelectron spectrometer was used to acquire X-ray photoelectron spectra (XPS-spectra). Anode voltage and emission current for the X-ray tube were 13 kV and 13 mA. To examine the optical properties, a diffuse reflectance UV-vis absorption spectrophotometer was used.

2.3 Evaluation of Photocatalytic Efficiency

The reaction was photocatalyzed by a 75 W Xe lamp in a quartz cold trap in a multilocation cylindrical reaction vessel under ambient cooling. Figure 1 illustrates the experimental setup for the photocatalytic degradation process with (a) Xenon lamp source, (b) incident light, (c) fan fan to keep sample chill, (d) water-cooling exhaust, (e) cooling-water intake, (f) beaker, (g) magnetic stirrer to mix things up, and (h) magnetic agitator to keep sample all moving. The reaction was carried out by adding 1.0 g of $CaFe_2O_4$ to 50 mL of MB. Before illumination, solutions were agitated for 2 h for photocatalyst-MB adsorption equilibrium. In 5 mL of solution, it was mixed and centrifuged. Supernatant absorption was measured at 665 nm using UV-vis spectrophotometers. Figure 1 depicts a Xenon lamp, incident light, fan, cooling-water outlet, cooling-water input, beaker, magnetic stirrer, and magnetic agitator. Degradation efficiency (De) was calculated using Eq(1), where A_0 and A are the initial and final maximum absorbances, respectively. The experiment of photocatalytic degradation was run for 30 min in the dark and for 160 min in next-to-no light. A simulated solar light (HAL-320W, Asahi spectra) was used as a light source to provide an irradiation intensity of 100 mW/cm^2 from the top of the solution.

$$De = \frac{(A_0 - A)}{A_0} \times 100\% \quad (1)$$

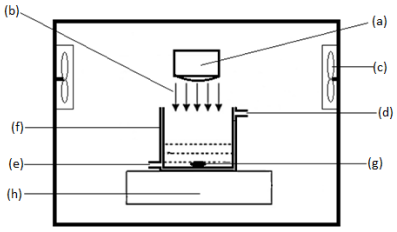

Figure 1: The schematic for the catalyst preparation and performance investigation

3. Results and discussions

3.1 Catalyst characterization

3.1.1 XRD analysis

The XRD patterns of catalyst (c-h) and precursor (a, b) samples that were calcined at various temperatures are shown in Figure 2. The samples were (a) $Ca(NO_3)_24H_2O$, (b) $Fe(NO_3)_39H_2O$, and (c) $CaFe_2O_4$ at (a) 450°C, (d) 600°C, (e) 700°C, (f) 800°C, (g) 900 °C, and (h) 1050 °C. The material was calcined at 450 and 600 °C, and diffraction patterns reveal it is amorphous. Above this temperature, the first desirable phase nuclei develop. Calcined at 800, 900, and 1050 °C, the samples were pure $CaFe_2O_4$ and nicely crystalline. The synthesis procedure produced the required phase at 800–1050 °C. The result shows that $CaFe_2O_4$ orthorhombic structure is comparable with JCPDS Card No. 74-2136. It agrees with peaks in literature (Khanna & Verma, 2013). Nanocrystallites arise as diffraction peaks expand. XRD patterns may be seen in the precursor's $Ca(NO_3)_24H_2O$, $Fe(NO_3)_39H_2O$, and $CaFe_2O_4$. Figure 3 shows how calcination temperatures affected crystallite sizes during catalyst preparation. This figure shows that amorphous materials crystallized at 700 °C and increased their crystallite sizes by 80% at 800 °C. Size increments were constant until 900°C, then increased again to 52 nm at 1,050 °C. Growth processes fluctuate with crystallite size. The central peaks of the diffraction pattern of the CaFe2O4 structure are located like (Guo et al., 2021) where planes with space group Pnma and JCPDS # 32–0168 are involved. Based on the literature, the crystallographic structure is correct. The XRD pattern of $CaFe_2O_4$ shows peaks that indicate the successful fabrication of the heterojunctions.

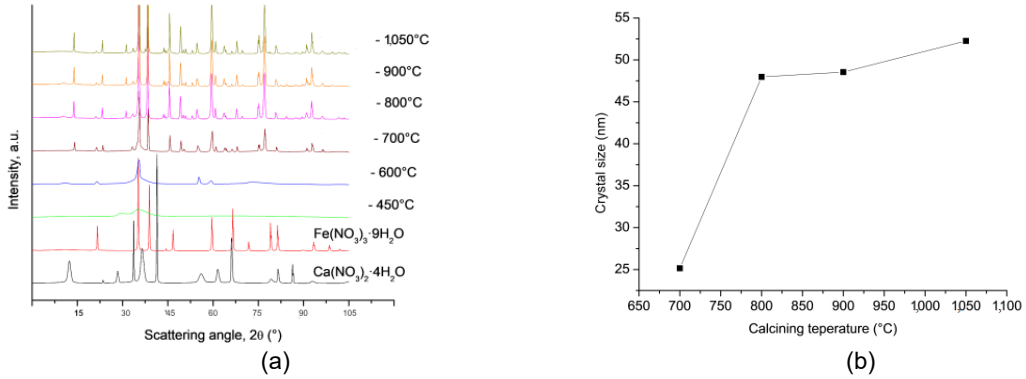

Figure 2: The XRD results with (a) the spectra of samples undergone calcination of 10 h; (b) The relationship between crystallite dimensions and temperature

3.1.4 TGA analysis

Figure 3 depicts the calcium ferrite heat degradation TGA curve. Physical water loss from nanoparticle surfaces caused samples (a) and (b) to lose weight between 50 and 250 °C. Sample (a) from the calcined at 450°C had outstanding TGA behavior. Due to crystallized water and NOx, it lost 2% and 5% of its weight between 250 and 450 °C (x = 1, 2) (Barati, 2009), and 5.8% (450–900 °C) from impurity and unreacted precursor removal (Khanna & Verma, 2013). For the six mixes in (a)–(f), the weight losses for high-temperature calcined materials decreased progressively, with 13.3, 9.86, 6.47, 3.47, 2.11, and 0.74%. Because catalysts calcined at 700°C were generally free of crystal water, NOx, and unreacted precursors, this trend was observed. Figure 3 shows that catalysts calcined at 800°C had little weight loss and enhanced stability. XRD patterns show that higher temperature calcination of calcium ferrite nanoparticles enhances crystallization stability (Figure 2).

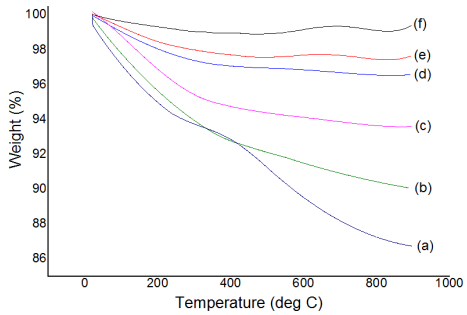

Figure 3: TGA curves at calcination temperatures on (a) 450°C, (b) 600°C, (c)700°C, (d) 800°C, (e) 900°C, and (f) 1,050°C temperature

3.1.5 XPS analysis

XPS spectra assess binding energy (eV) to determine species concentrations, including composite photocatalysts, and if there are impurities or a uniform distribution of components. Fe 2p, O1s, and Ca 2p XPS spectra are displayed in Figure 4. Fe 2p1/2's primary signal is at 724.3 eV, and Fe 2p3/2's is at 710.9 eV, corresponding to the literature data (Lu et al., 2022). Fe_2O_3 and FeO show substantial shake-up satellites in their Fe 2p spectra at 718 eV and 713 eV, respectively. O1's core-level XPS spectra are displayed in Figure 4(b). At 529 and 531 eV, the spectrum exhibits two significant peaks. An oxygen molecule with a well-ordered lattice has a lower binding energy state. In contrast, an oxygen molecule with a more prominent binding energy peak at 531 eV might be connected to a different surface oxide or structural faults in the catalyst (Wang et al., 2019). Bulk CaO contributes 531 eV to O1. The detailed structure of the most substantial calcium peak is shown in Figure 5 (c). All spectra show contributions from Ca 2p3/2 and Ca 2p1/2. The Ca2p3/2 and Ca2p1/2 peaks are 346.4 and 350.4 eV, respectively. The Ca2p3/2 peak indicates pure Ca. Calcium oxide with a lower valence than CaO may be found alongside the metallic phase. As expected, the significant components in $CaFe_2O_4$ were Fe, Ca and O.

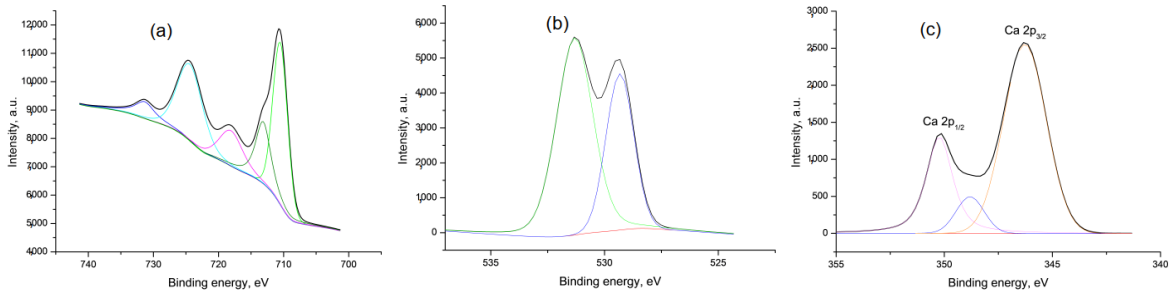

Figure 4: XPS analysis for spectra with high resolution on (a) Fe 2p, (b) O 1s, (c) Ca 2p

3.1.6 UV-vis spectra analysis

Figure 5 depicts the CaFe2O4 powder samples' UV-vis absorption between 700 and 1,050 °C. The sample calcined at 1,050 °C had absorption band edges at 728 nm that were larger than those at 700 °C (which are thought to be 620 nm). The ideal absorption edge for visible light photocatalysis is 620 nm. As a result, the optical characteristics of $CaFe_2O_4$ calcined at 700 °C are suitable and necessary for creating a high-efficiency photocatalyst. These bandgaps are consistent with the previously reported values (Keerthana et al., 2022). Reported band gaps for $CaFe_2O_4$ samples were 1.5–1.9 eV (Kamali et al., 2021). The lift in this range influences the photocatalytic performance of the sample (Guo et al., 2021). The blue shift may be assigned because of the quantum effect. Meanwhile, the bandgap value influences the photocatalytic degradation of MB. Figure 6's measurement of MB activity demonstrated this. The crossing point regularly shows the optical band gap respectively referred to formula Eg = 1240/wavelength (Mehrabanpour et al., 2022). 700 °C-calcined $CaFe_2O_4$ showed a band gap of 2 eV, higher than other samples (Table 1). $CaFe_2O_4$'s tiny band gap should demonstrate this. The result shows that due to the increased activity of NCs as photocatalysts due to enhanced light absorption and reduced photogenerated e/h+ pair recombination due to heterojunction formation (Syed et al., 2021). The calcination effect showed stronger absorption in the visible light region, indicating that the

heterojunctions can effectively utilize the light energy generated within the visible region of the electromagnetic spectrum and generate more electron–hole pairs for redox reactions.

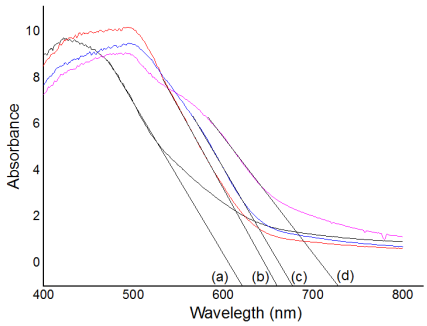

Figure 5: Spectrum UV-vis absorption at calcination temperatures: (a) 700°C, (b) 800°C, (c) 900°C, and (d) 1,050°C

Table 1. Band gap energy of $CaFe_2O_4$ calcined at various temperatures from its UV-vis absorption spectrum

Catalyst $CaFe_2O_4$ (°C)	Band gap energy	
	E(Ev)	λ (nm)
700	2.00	620
800	1.88	660
900	1.83	677
1050	1.70	728

3.1.7 Photocatalytic activities

An efficient photocatalytic reaction was performed at 27 °C to determine the influence of $CaFe_2O_4$ photocatalyst on MB adsorption. Photocatalytic degradation does not occur in a blank experiment without photocatalyst powder. Calcinating temperatures affect its capacity to break down MB from aqueous waste solutions. The photocatalytic powder must have a specific crystalline size and area to remove cationic hazardous waste (MB) from wastewater. Figure 6 shows how catalyst samples calcined at various temperatures degrade to 50 and 75 ppm MB. A $CaFe_2O_4$ photocatalyst could use visible light irradiation to degrade more than 50% of the dye in an aqueous solution due to the photocatalyst's ability to form enough electron holes (Keerthana et al., 2022). The carbon material amplified more active sites for recombination, and an almost complete light source was used energetically. The degradation percentage was obtained after 160 minutes of irradiation of $CaFe_2O_4$ with visible light.

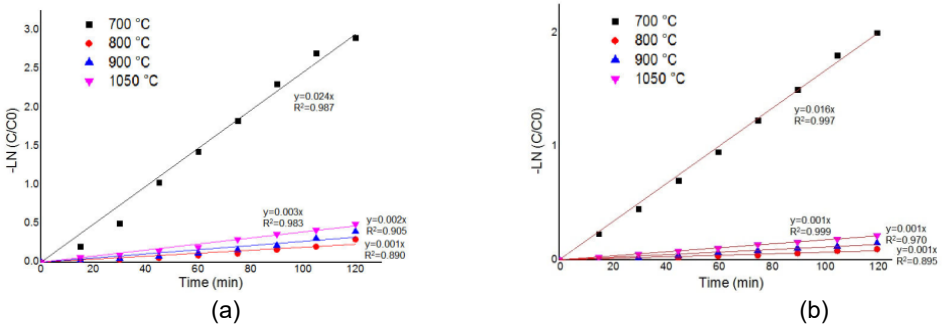

Figure 6: MB activity assessment at (a) 50 ppm and (b) 75 ppm

4. Conclusions

Sol-gel calcination at varying temperatures produced nanostructured $CaFe_2O_4$ photocatalysts; 10 h of calcination at 1,050°C enhanced catalyst structure and activity. XRD indicated a constant 48–52 nm crystal size at 800-1,050°C. BET found 9.89–0.54 m^2/g surface areas. Thermal and XPS spectra show no organic contaminants or unreacted precursors. Photocatalytic $CaFe_2O_4$ powder destroyed MB dyes. Quantity impacted

photocatalysis. ion flaws may split photogenerated electrons and holes. XRD confirmed that nanosized $CaFe_2O_4$ particles significantly improved photocatalytic activity. $CaFe_2O_4$ photocatalysts degrade MB well in water.

Acknowledgments

The author would like to express his gratitude DRB-HICOM University for its ongoing support of this effort.

References

Antony J., Gonzalez S.V., 2023, Silica-modified bismutite nanoparticles for enhanced adsorption, Catalysis Today. 52, 11.

Aslam Z., Saifu Rahman R., 2022, Photocatalytic response of CuCdS2 nanoparticles under solar irradiation, Chemical Physics Letters, 2, 804.

Barati M.R., 2009, Characterization of MgCuZn ferrite powders synthesized, Journal of Sol-Gel Science and Technology, 52, 171–178.

Benites-Alfaro E., 2022, Bacterial Treatment of Wastewater by Hydrodynamic Cavitation, Chemical Engineering Transactions, 96, 205–210.

Bidu J.M., 2023, Textile wastewater treatment: Influence of domestic wastewater, South African Journal of Chemical Engineering, 43, 112–121.

Glazkova E.A., 2022, Copper ferrite/copper oxides by electric explosion of wires, Materials Science and Engineering B: Advanced Technology, 283, 11.

Guo L., 2021, Molten salt-assisted shape modification of CaFe2O4 nanorods, Optical Materials, 119, 12.

Jarusheh H.S., Yusuf A., 2022, Technologies in water treatment using , Journal of Environmental Chemical Engineering, 10, 5.

Jayalakshmi R., 2022, Removal of Methylene Blue dye from textile wastewater using vertical flow constructed wetland, Materials Today: Proceedings, 7, 56.

Kamali M., Sheibani S., 2021, Magnetic MgFe2O4–CaFe2O4 S-scheme photocatalyst, Journal of Environmental Management, 290,11.

Keerthana SP., 2022, Investigation of g-C3N4 ratio on CaFe2O4 to remove toxic pollutants from wastewater, Journal of Hazardous Materials Advances, 7, 100.

Khanna L., Verma N.K., 2013, Synthesis, characterization and in vitro cytotoxicity study of calcium ferrite nanoparticles, Materials Science in Semiconductor Processing, 16, 1842–1848.

Khosroshahi N., 2022, Mechanochemical synthesis of ferrite/MOF nanocomposite, Journal of Photochemistry and Photobiology A: Chemistry, 431, 11.

Kousar T., Aadil M., 2022, Temperature controlled synthesis of Co-Ni mixed ferrite nanostructure for the mineralization of azo dye: A novel and facile approach, Journal of Alloys and Compounds, 923,33.

Kukwa D.T., Chetty M., 2022, Biomass Production and Simultaneous Minerals Sequestration from Brewery Wastewater, Chemical Engineering Transactions, 96, 475–480.

Lu Y., Mushtaq N., 2022, Improved self-consistency and oxygen reduction activity of CaFe2O4 for protonic ceramic fuel cell by porous NiO-foam support, Renewable Energy, 199, 1451–1460.

Mehrabanpour N., 2022, A comparative photocatalytic activity between PbS NPs and PbS-clinoptilolite towards Cefotaxime, Solid State Sciences, 131,23.

Phakathi N.A., 2022, Photocatalytic Degradation of Tetracycline using Visible-light-driven Porous g- C3N4 Nanosheets Catalyst, Chemical Engineering Transactions, 96, 391–396.

Sanchez-Albores R., 2022, Microwave-assisted biosynthesis of ZnO-GO particles using orange peel extract, Journal of Environmental Chemical Engineering, 10, 108.

Syed A., 2021, Enhanced visible light driven photocatalytic activity of CaFe2O4 doped CdO heterojunction, Optical Materials, 113, 11.

Tuna O., 2023, Enhanced visible-light-assisted peroxymonosulfate activation, Materials Research Bulletin, 159, 13.

Wang J., 2019, In situ of α-Fe2O3/CaFe2O4 p-n heterojunction, Advanced Powder Technology, 30, 590.